Article

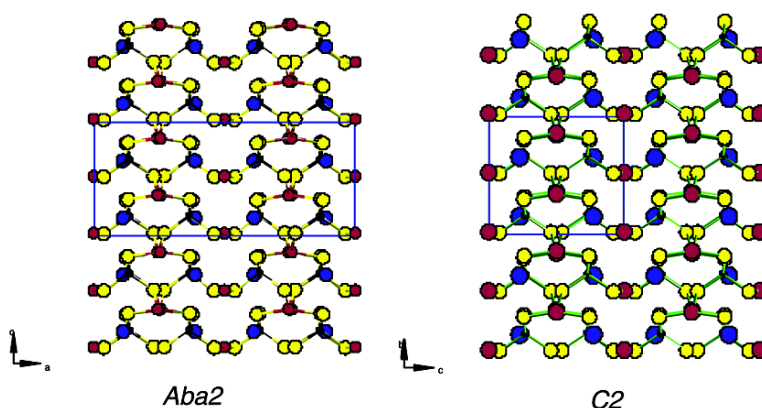# α- and β-AHgMS (A = K, Rb; M = Ge, Sn): Polar Quaternary Chalcogenides with Strong Nonlinear Optical Response

J.-H. Liao, G. M. Marking, K. F. Hsu, Y. Matsushita, M. D. Ewbank,
R. Borwick, P. Cunningham, M. J. Rosker, and M. G. Kanatzidis

Aba2　　　*C2*

More About This Article

Additional resources and features associated with this article are available within the HTML version:

- Supporting Information
- Links to the 7 articles that cite this article, as of the time of this article download
- Access to high resolution figures
- Links to articles and content related to this article
- Copyright permission to reproduce figures and/or text from this article

View the Full Text HTML

α- and β-A$_2$Hg$_3$M$_2$S$_8$ (A = K, Rb; M = Ge, Sn): Polar Quaternary Chalcogenides with Strong Nonlinear Optical Response

J.-H. Liao,[†] G. M. Marking,[†] K. F. Hsu,[†] Y. Matsushita,[†] M. D. Ewbank,[‡] R. Borwick,[†] P. Cunningham,[‡] M. J. Rosker,[‡] and M. G. Kanatzidis*,[†]

Contribution from the Department of Chemistry and Center for Fundamental Materials Research, Michigan State University, East Lansing, Michigan 48824-1322, and Rockwell International Science Center, Thousand Oaks, California 91360

Received January 10, 2003; Revised Manuscript Received April 20, 2003; E-mail: kanatzid@cem.msu.edu

Abstract: The closely related phases α- and β-A$_2$Hg$_3$M$_2$S$_8$ (A = K, Rb; M = Ge, Sn) have been discovered using the alkali polychalcogenide flux method and are described in detail. They present new structure types with a polar noncentrosymmetric crystallographic motif and strong nonlinear second-harmonic generation (SHG) properties. The α-allotropic form crystallizes in the orthorhombic space group *Aba*2 with *a* = 19.082(2) Å, *b* = 9.551(1) Å, *c* = 8.2871(8) Å for the K$_2$Hg$_3$Ge$_2$S$_8$ analogue, and *a* = 19.563(2) Å, *b* = 9.853(1) Å, *c* = 8.467(1) Å for the K$_2$Hg$_3$Sn$_2$S$_8$ analogue. The β-form crystallizes in the monoclinic space group *C*2 with *a* = 9.5948(7) Å, *b* = 8.3608(6) Å, *c* = 9.6638(7) Å, β = 94.637° for the K$_2$Hg$_3$Ge$_2$S$_8$ analogue. The thermal stability and optical and spectroscopic properties of these compounds are reported along with detailed solubility and crystal growth studies of the α-K$_2$Hg$_3$Ge$_2$S$_8$ in K$_2$S$_8$ flux. These materials are wide gap semiconductors with band gaps at ∼2.40 and ∼ 2.64 eV for the Sn and Ge analogues, respectively. Below the band gap the materials exhibit a very wide transmission range to electromagnetic radiation up to ∼14 μm. α-K$_2$Hg$_3$Ge$_2$S$_8$ shows anisotropic thermal expansion coefficients. SHG measurements, performed with a direct phase-matched method, showed very high nonlinear coefficient d_{eff} for β-K$_2$Hg$_3$Ge$_2$S$_8$ approaching 20 pm/V. Crystals of K$_2$Hg$_3$Ge$_2$S$_8$ are robust to air exposure and have a high laser-damage threshold.

Introduction

The use of nonlinear optics (NLO) to adapt lasers to wavelength-specific applications has highlighted the need for new, efficient, and damage-resistant NLO materials. Well-developed crystals exist for frequency conversion of such lasers as the neodymium:yttrium aluminum garnet (Nd:YAG); however, new materials with higher conversion efficiencies and improved durability remain highly desirable.[1] The need is particularly acute in the midwave (2−5 μm) and far-wave (>5 μm) infrared regions in which applications have been demonstrated using optical parametric oscillation (OPO), but relatively few materials combine the required nonlinearity, good optical transmissivity, and high resistance to optical damage in this region.[2] The non-centrosymmetric polar characteristics and simultaneous transmission of long wavelength radiation required of such crystals

point to complex chalcogenides as a potential source of NLO materials.

As a source of new NLO materials, quaternary chalcogenides are attractive due to a variety of acentric arrangements resulting from the combination of two kinds of metal centers with different size, coordination preference, and packing characteristics.[3] Previously, we reported a series of alkali metal, quaternary chalcogenides based on the tetrahedral anions [SnS$_4$]$^{4-}$ and [GeS$_4$]$^{4-}$ stabilized in polysulfide fluxes.[4,5] In a large number of cases, phases with these anions tend to be noncentrosymmetric, as, for example, Na$_{0.5}$Pb$_{1.75}$GeS$_4$,[6] Li$_{0.5}$Pb$_{1.75}$GeS$_4$,[5] Ba$_3$Cd(SnS$_4$)$_2$,[7] Ba$_6$CdAg$_2$(SnS$_4$)$_4$,[6] KLnGeS$_4$,[8] KInGeS$_4$,[9] KGaGeS$_4$,[10] Eu$_2$GeS$_4$,[11] and BaAg$_2$GeS$_4$.[12] It is possible that

† Michigan State University.

‡ Rockwell International Science Center.

(1) (a) Keszler, D. A. *Curr. Opin. Solid State Mater. Sci.* **1996**, *1(2)*, 204−211 (b) Becker, P. *Adv. Mater.* **1998**, *10(13)*, 979.

(2) (a) Rotermund, F.; Petrov, V.; Noack, F. *Optics Commun.* **2000**, *185*, 177−183. (b) Zhao, B. J.; Zhu, S. F.; Li, Y. D.; Yu, F. L.; Li, Q. F.; Li, Z. H.; Zhu, X. H.; Shao, S. Y.; Lin, J. *Optic. Eng.* **1999**, *38(12)*: 2129−2133 (c) Apollonov, V. V.; Lebedev, S. P.; Komandin, G. A.; Shakir, Y. A.; Badikov, V. V.; Andreev, Y. M.; Gribenyukov, A. I. *Laser Phys.* **1999**, *9*, 1236−1239 (d) Vodopyanov, K. L.; Maffetone, J. P.; Zwieback, I.; Ruderman, W. *Appl. Phys. Lett.* **1999**, *75*, 1204−1206 (e) Gorobets, V. A.; Petukhov, V. O.; Tochitskii, S. Y.; Churakov, V. V. *J. Optic. Technol.* **1999**, *66*, 53−57.

(3) (a) Kanatzidis, M. G.; Liao, J.-H.; Marking, G. A. Alkali Metal Quaternary Chalcogenides and Process for the Preparation Thereof. United States Patent 5,614,128. (b) Kanatzidis, M. G.; Liao, J.-H.; Marking, G. A. Alkali Metal Quaternary Chalcogenides and Process for the Preparation Thereof. United States Patent 5,618,471.

(4) Liao, J.-H.; Kanatzidis, M. G. Submitted for publication.

(5) (a) Aitken, J. A.; Larson, P.; Mahanti, S. D.; Kanatzidis, M. G. *Chem. Mater.* **2001**, *13*, 4714−4721. (b) Matsushita, Y.; Kanatzidis, M. G. *Z. Naturforsch. B* **1998**, *53b*, 23−30.

(6) Aitken, J. A.; Marking, G. A.; Evain, M.; Iordanidis, L.; Kanatzidis, M. G. *J. Solid State Chem.* **2000**, *153*, 158−169.

(7) Teske, C. L. Z. *Anorg. Allg. Chem.* **1985**, *522*, 122−130.

(8) (a) Wu, P.; Ibers, J. A. *J. Solid State Chem.* **1993**, *107*, 347. (b) Gauthier, G.; Guillen, F.; Jobic, S.; Deniard, P.; Macaudiere, P.; Fouassier, C.; Brec, R. *Compt. Rend. Acad. Sci. Ser. II* **1999**, *2*, 611.

(9) Klemm, W.; Sodomann, H.; Langmesser, P. Z. *Anorg. Allg. Chem.* **1939**, *241*, 281−304.

the use of these tetrahedral anions in combination with heavy elements may increase the odds of forming acentric phases.[13] We report here the synthesis, crystal growth, spectroscopic characterization, thermal stability, and preliminary NLO properties of the new compounds α- and β-$K_2Hg_3Ge_2S_8$ and α- and β-$K_2Hg_3Sn_2S_8$. In an earlier publication, we reported results on the centrosymmetric versions of these systems $A_2Hg_3M_2S_8$ (A = Rb, Cs; M = Ge, Sn) and γ-$Rb_2Hg_3M_2S_8$ (M = Ge, Sn).[14]

Both the α- and β-forms possess polar noncentrosymmetric structures that adopt the *Aba*2 and *C*2 space groups, respectively. The Rb analogues are also described. These materials have a unique structure, possess high infrared transmission, and exhibit strong second-harmonic generation (SHG), particularly in the midwave and far-wave infrared region. α- and β-$K_2Hg_3Ge_2S_8$ and α- and β-$K_2Hg_3Sn_2S_8$ easily crystallize in millimeter-sized crystals with high spectral transparency and high laser damage threshold.

Experimental Section

Reagents. Sn metal was ~325 mesh, 99.8% purity; Ge metal was ~100 mesh, 99.99% purity; and sublimed sulfur was 99.5−100% purity. HgS powder was from J. T. Baker Inc., Phillipsburg, NJ. A_2S (A = K, Rb) starting materials were prepared by the stoichiometric reaction of A and S in liquid ammonia.

Synthesis. α-$K_2Hg_3Ge_2S_8$ (I) The reaction of Ge (0.018 g, 0.25 mmol), HgS (0.087 g, 0.38 mmol), K_2S (0.055 g, 0.50 mmol), and S (0.128 g, 4.00 mmol) at 400 °C for 4 d upon cooling at a rate of 4 °C/h afforded yellow crystals of **I** and a very small amount of HgS crystals. After washing with degassed DMF, the yield of **I** was 0.083 g (64%, based on Ge). The product is stable in air and insoluble in water and common organic solvents.

α-$K_2Hg_3Sn_2S_8$ (II) A mixture of Sn powder (0.030 g, 0.25 mmol), HgS powder (0.116 g, 0.499 mmol), K_2S (0.055 g, 0.50 mmol), and S (0.128 g, 4.00 mmol) was sealed in an evacuated glass ampule and heated at 400 °C for 4 d and then cooled to room temperature at 4 °C/h. The product was washed with degassed DMF and dried with acetone and ether. Yellow crystals of **II** and small amounts of orange-brown square planar crystals and red HgS crystals (less than 5%) were obtained. The yellow crystals (69% yield based on Sn) are insoluble in water and common organic solvents.

β-$K_2Hg_3Ge_2S_8$ (III). Method A. The nearly direct combination reaction of Ge (0.073 g, 1.01 mmol), HgS (0.349 g, 1.50 mmol), K_2S (0.055 g, 0.50 mmol), and excess S (0.129 g, 4.02 mmol) was heated to 520 °C over 6 h, held at that temperature for 1 h, and cooled to 480 °C at a rate of 1 °C/h. The product was washed with degassed methanol, deionized water, and carbon disulfide to remove excess sulfur and then dried with acetone and ether. A pure, yellow microcrystalline phase was obtained, and powder X-ray diffraction indicated that it was β-$K_2Hg_3Ge_2S_8$. The yellow product (mainly single crystals) is stable in air and insoluble in water and common organic solvents.

Method B. This is a faster procedure. Typically the reaction vessels were heated in tube furnaces up to 400−500 °C over a period of 8−12 h, held at that temperature for 2−4 days, and cooled to about 200 °C at a rate of 4 °C/h. Excess flux was dissolved using methanol under nitrogen atmosphere, and the crystals were washed with water to dissolve any ternary K−Ge−S phase present and then dried with acetone and ether. Excess sulfur was dissolved using carbon disulfide. All of the time periods in the temperature profile can be shortened

without drastically reducing the yield from 85%, but the product becomes increasingly microcrystalline.

β-$K_2Hg_3Sn_2S_8$ (IV). A mixture of Sn powder (0.030 g, 0.25 mmol), HgS powder (0.089 g, 0.38 mmol), K_2S (0.056 g, 0.50 mmol), and S (0.130 g, 4.06 mmol) was sealed in an evacuated glass ampule and heated at 400 °C for 4 d and then cooled to 160 °C at 80 °C/h. The product was washed with degassed methanol and deionized water and then dried with acetone and ether. Large yellow crystals of **IV** and a few small brown square planar crystals were obtained (>70% yield). Powder X-ray diffraction indicated that the yellow crystals were substantially β-phase but α-phase was also present. The yellow crystals are insoluble in water and common organic solvents.

β-$Rb_2Hg_3Ge_2S_8$ (V) and β-$Rb_2Hg_3Sn_2S_8$ (VI). The synthesis of these isostructural compounds is similar to those for **I** and **II** above. β-$Rb_2Hg_3Ge_2S_8$ was prepared with a slight excess of HgS powder (0.145 g, 0.63 mmol) and heated at 500 °C for 4 d and cooled to 200 °C at 4 °C/h, yielding small yellow crystals of **V** as a nearly pure material. β-$Rb_2Hg_3Sn_2S_8$ was also prepared as light yellow crystals with an slight excess of HgS (0.144 g, 0.62 mmol), using the same heating profile. Both products are stable in air and insoluble in water and common organic solvents.

β-$K_{1.6}Rb_{0.4}Hg_3Ge_2S_8$ (VII). A mixture of Ge (0.018 g, 0.25 mmol), HgS (0.118 g, 0.51 mmol), K_2S (0.041 g, 0.37 mmol), Rb_2S (0.025 g, 0.12 mmol), and S (0.130 g, 4.05 mmol) was heated at 400 °C for 3 d and then cooled to 385 °C over a 5 d period and then to 165 °C at a rate of 2 °C/h. Large platelike yellow crystals of **VII** (>75% yield based on Ge), a trace amount of HgS, and water-soluble dark material were obtained. The product is stable in air and insoluble in water and common organic solvents. SEM/EDS analysis indicated an approximate K/Rb ratio of ~4/1.

Crystal Growth of α-$K_2Hg_3Ge_2S_8$, β-$K_2Hg_3Ge_2S_8$ and α-$K_2Hg_3Sn_2S_8$. *Recrystallization from K_2S_x Fluxes.* Quantities of α-K_2-$Hg_3Ge_2S_8$ and α-/β- mixtures of $K_2Hg_3Ge_2S_8$ were prepared for recrystallization experiments. Additional combinations of the α/β-phase mixture with K_2S_3 in 1:1, 1:5, and 1:20 ratios were heated to 420 °C over a 25 h period, isothermed at 420 °C for 3 d, and rapidly cooled to 170 °C in 3 h. These rapidly cooled reactions did not yield any $K_2Hg_3Ge_2S_8$. Then the α/β-mixture was combined with K_2S_3 flux in a 1:16 ratio and heated at 400 °C for 2 d and cooled to low temperature at 4 °C/h. After isolation by washing with degassed DMF and drying with ether and acetone, the product was observed to be medium-sized crystals. The material was determined to be pure β-$K_2Hg_3Ge_2S_8$ through X-ray diffraction.

α-$K_2Hg_3Ge_2S_8$ could also be recrystallized from K_2S_8 flux in a 1:1 ratio. In this experiment, 0.20 g (1.9 × 10⁻⁴ mol) of α-$K_2Hg_3Ge_2S_8$ powder was mixed with 1.9 × 10⁻⁴ mol of K_2S_8 (0.033 g of K_2S_3 and 0.03 g of S) and loaded in a Pyrex tube, which was flame-sealed under vacuum. It was heated slowly to 420 °C and kept there for 4 d and then cooled to 200 °C at a rate of 2 °C/h. The product was isolated by washing with DMF and dried with acetone and ether to yield 0.145 g of large (~3 mm in size) yellow platelike crystals of α-$K_2Hg_3Ge_2S_8$. Recrystallization reactions of α-$K_2Hg_3Sn_2S_8$ powder in K_2S_8 flux under the same conditions also gave relatively large millimeter-sized crystals.

Mixtures of α-$K_2Hg_3Ge_2S_8$ powder and K_2S_8 flux in 1:3 and 1:5 ratios under the same reaction conditions also gave millimeter-sized crystals. When more K_2S_8 was used, however, the crystal size and yield were smaller. More basic flux conditions (created by increasing the K_2S fraction) were also studied using the overall compositions "$K_{16}Hg_{3.5}Ge_2S_{36}$" and "$K_{16}Hg_2Sn_2S_{36}$". These reaction mixtures were initially heated to 500 °C over a 5 h period, held there for 45 h, and subsequently cooled at 4 °C/h to 180 °C followed by cooling to 50 °C in 12 h. The desired noncentrosymmetric phases had apparently decomposed under these more basic conditions and instead the products were large black crystals of $K_2Hg_6S_7$[15] in the first reaction and a mixture of $K_2Hg_6S_7$ and large brown chunks of K_2HgSnS_4[16] in the second.

(10) Krebs, B. *Angew. Chem., Int. Ed. Engl.* **1983**, 22, 113−134.
(11) Tampier, M.; Johrendt, D. *J. Solid State Chem.* **2001**, *158(2)*, 343−348.
(12) Müller, D.; Hahn, H. *Z. Anorg. Allg. Chem.* **1978**, *438*, 258.
(13) Halasyamani, P. S.; Poeppelmeier, K. R. *Chem. Mater.* **1998**, *10*, 2753−2769.
(14) Marking, G. A.; Hanko, J. A.; Kanatzidis, M. G. *Chem. Mater.* **1998**, *10*, 1191−1199.

Table 1. Summary of Crystallographic Data and Refinement Details for α- and β-$A_2Hg_3M_2S_8$, (A = K, Rb; M = Sn, Ge)

	I	II	III	VII
formula	α-$K_2Hg_3Ge_2S_8$	α-$K_2Hg_3Sn_2S_8$	β-$K_2Hg_3Ge_2S_8$	β-$K_{1.6}Rb_{0.4}Hg_3Ge_2S_8$
fw	1081.63	1173.83	1081.63	1099.71
a, Å	19.082(2)	19.563(2)	9.5948(7)	9.649(5)
b, Å	9.551(1)	9.853(1)	8.3608(6)	8.393(2)
c, Å	8.2871(8)	8.467(1)	9.6638(7)	9.720(2)
α, deg	90.0	90.0	90	90.0
β, deg	90.0	90.0	94.637(1)	95.08(3)
γ, deg	90.0	90.0	90	90.0
Z, V (Å^3)	4, 1510.3(4)	4, 1630.2(6)	2, 772.7(2)	2, 784.0(5)
space group	$Aba2$	$Aba2$	$C2$	$C2$
d_{calc}, g/cm^3	9.514	9.555	9.322	4.658
crystal size, mm	0.14 × 0.14 × 0.02	0.20 × 0.05 × 0.05	0.16 × 0.10 × 0.05	0.23 × 0.28 × 0.39
temp (°C)	23	23	23	23
radiation	Mo Kα	Mo Kα	Mo Kα	Mo Kα
diffractometer	Smart CCD	Smart CCD	Smart CCD	Rigaku AFC6S
μ(Mo Kα), mm^{-1}	71.889	65.283	70.440	71.21
$2\theta_{max}$, deg	57.2	56.5	56.9	55
no. of data collected	2904	4712	2380	1027
no. of unique data	1510	1638	1616	969
no. of variables	70	65	70	3.8/4.6
final R_1/wR_2, %^{a}	7.5/18.7	4.3/11.3	4.2/11.1	4.6/4.7

^{a} $R_1 = \sum ||F_o| - |F_c||/\sum |F_o|$. $wR_2 = \{\sum[w(F_o^2 - F_c^2)^2]/\sum w[(F_o^2)^2]\}^{1/2}$.

Crystal Growth from Slow Cooling. Large, but not optical quality, crystals of α-$K_2Hg_3Ge_2S_8$ (up to 4 × 5 × 8 mm^3) and α-$K_2Hg_3Sn_2S_8$ (up to 4 × 4 × 5 mm^3) were prepared from flux reactions using the overall stoichiometry "$K_8Hg_4M_2S_{40}$", where M = Ge or Sn. The mixtures were heated to 500 °C over an 8 h period and then cooled to 400 °C in 2 h. They were held at the 400 °C for 6 d and subsequently cooled at 1 °C/h to 200 °C followed by cooling to 50 °C in 2 h.[17]

Physical Measurements. The instruments and experimental setups for infrared spectroscopy, SEM/EDS quantitative microprobe analysis, and UV/vis/near-IR optical diffuse spectroscopy are the same as those described earlier.[14]

Thermal Analyses. Differential thermal analyses (DTA) were performed using a computer-controlled Shimadzu DTA-50 thermal analyzer. Amounts of 10−60 mg of sample were sealed in quartz tubes under vacuum and heated at 10 °C/min to a temperature of 600 °C, isothermed for 10 min, and finally cooled to 100 °C at 10 °C/min. Samples were cycled through this heating profile from one to three times, and empty quartz tubes equal in mass to the sample were present on the reference side of the detector. Thermogravimetric analysis (TGA) was performed using a computer-controlled Shimadzu TGA-50 analyzer. A 30 mg sample was placed in a small quartz bucket and heated in a flowing nitrogen atmosphere at 5 °C/min. The DTA and TGA samples were visually inspected and then analyzed by X-ray diffraction after the experiments.

X-ray Crystallography. X-ray powder diffraction patterns were used for the purpose of phase characterization and identification. The X-ray powder diffraction patterns were recorded with a Phillips XRD-3000 controlled by PDP 11 computer and operating at 40 kV/35 mA. Graphite monochromatic Cu Kα radiation was used. To assess phase purity, d spacings obtained from X-ray powder diffraction (XRD) measurements of products were compared with those calculated from the atomic coordinates determined from the single-crystal X-ray data.

Single crystals of α-$K_2Hg_3Ge_2S_8$ (**I**), α-$K_2Hg_3Sn_2S_8$ (**II**), and β-$K_2Hg_3Ge_2S_8$ (**III**) were mounted on the tip of glass fibers. The data were collected on a Bruker SMART Platform CCD diffractometer with graphite-monochromatized Mo Kα radiation. The SMART[18] software was used for the data acquisition and SAINT[19] for the data extraction and reduction. The absorption correction was performed with SADABS.[20] Structure solution and refinement were performed with the SHELXTL package of crystallographic programs.[21]

The single-crystal X-ray diffraction data of **VII** were collected on a Rigaku AFC6S four-circle diffractometer. Measuring three standard reflections, periodically every 150 reflections for all the data sets, monitored the stability of the experimental setup and crystal integrity. No significant decay was observed during the data collections. The structures were solved with direct methods (SHELXS-86), and were refined by the full-matrix least-squares technique available in TEXSAN.[22] An empirical absorption correction was applied to all the data (based on ψ scans). The enantiomorphism of **III** was verified with Flack parameter 0.07(1). The crystallographic data and detailed information of structure solution and refinement are listed in Table 1. Atomic coordinates and equivalent isotropic thermal parameters are given in Table 2, respectively.

NLO Measurements and Direct Phase Matching (DPM). Measurements were made on both powder and single crystal samples. Glass vials containing the powder were placed in front of a pulsed Nd:YAG laser (1064 nm) and the characteristic green light at 532 nm coming from the sample was visually observed. Single crystals were ground into spheres and used for the DPM characterization according to a procedure described elsewhere.[23] For powder experiments in the infrared region a detector was used to measure SHG. Light from a LiNbO$_3$ optical parametric oscillator (OPO) (150 μJ at 3.5 μm) was focused onto the powder sample through a 50 mm CaF$_2$ lens. A half-elliptical mirror was used to collect the maximum amount of signal from the powder sample onto the detector. The powder sample in a 2 mm quartz cylindrical cell was placed at one focus of the half-elliptical mirror

(15) Axtell, E. A.; Park, Y.; Chondroudis, K.; Kanatzidis, M. G. *J. Am. Chem. Soc.* **1998**, *120*, 124−136.

(16) Marking, G. A.; Kanatzidis, M. G. Unpublished results.

(17) The initial heating to 500 °C presumably dissolved most (but not all) of the seed crystals that had formed. Upon holding at 500 °C for 2 d and subsequent cooling, material at 2−4 °C/h deposited on only remaining seeds, resulting in just a few large crystals. Much slower cooling (<0.1 °C/h) and/or longer isotherms should lead to still larger crystals. Similar experiments investigating the use of less K$_2$S$_x$ flux were performed using the overall nominal stoichiometry K$_4$Hg$_4$M$_2$S$_{20}$, where M = Ge or Sn, and the same heating and cooling profile. In this case, the resulting crystals (α-phase) were mostly 0.1−0.5 mm in each dimension.

(18) *SMART*; Siemens Analytical X-ray Systems, Inc.: Madison, WI, 1994.

(19) *SAINT*, Version 4; Siemens Analytical X-ray Systems, Inc.; Madison, WI, 1994−1996.

(20) *SADABS*, Version 4; Siemens Analytical X-ray Systems, Inc.; Madison, WI, 1994−1996.

(21) Sheldrick, G. M. *SHELXTL*, Version 5; Siemens Analytical X-ray Systems, Inc.: Madison, WI, 1994.

(22) TEXSAN-TEXRAY Structure Analysis Package, Molecular Structure Corporation (1985).

(23) Rosker, M. J.; Marcy, H. O. In *Novel Optical Materials and Applications*; Khoo, I. C., Simoni, F., Umeton, C., Eds.; John Wiley and Sons: New York, 1997; pp 175−204.

Table 2. Positional Parameters and Equivalent Isotropic Displacement (Å²) for α-$K_2Hg_3Ge_2S_8$ (I), α-$K_2Hg_3Sn_2S_8$ (II), β-$K_2Hg_3Ge_2S_8$ (III), and β-$K_{1.6}Rb_{0.4}Hg_3Ge_2S_8$ (VII)

		I					II		
atom	x	y	z	U_{eq}[a]	atom	x	y	z	U_{eq}
K	0.3886(5)	0.8012(9)	0.8517(11)	0.027(2)	K	0.3837(2)	0.7934(3)	0.8441(5)	0.030(1)
Hg(1)	0.5	1.0	0.4839(3)	0.022(1)	Hg(1)	0.5	1.0	0.4898(1)	0.023(1)
Hg(2)	0.2546(1)	0.5437(1)	0.6506(2)	0.025(1)	Hg(2)	0.2548(1)	0.5393(1)	0.6488(1)	0.029(1)
Ge	0.3652(2)	0.7885(3)	0.3385(4)	0.09(1)	Sn	0.3668(1)	0.7850(1)	0.3371(1)	0.014(1)
S(1)	0.2703(5)	0.7916(7)	0.4770(13)	0.017(2)	S(1)	0.2670(2)	0.7874(3)	0.4904(5)	0.021(1)
S(2)	0.4620(4)	0.7679(8)	0.4900(12)	0.015(2)	S(2)	0.4692(2)	0.7698(3)	0.4958(5)	0.020(1)
S(3)	0.3753(5)	0.4828(8)	0.6952(10)	0.014(2)	S(3)	0.3750(2)	0.4892(3)	0.6832(5)	0.019(1)
S(4)	0.1321(5)	0.5972(9)	0.6884(9)	0.015(2)	S(4)	0.1328(2)	0.5833(3)	0.6791(4)	0.018(1)

		III					VII		
atom	x	y	z	U_{eq}	atom	x	y	z	B_{eq}[b]
K	0.7843(4)	0.8483(4)	0.7714(4)	0.032(1)	A[c]	0.2124(4)	0.1520(6)	0.2270(4)	1.7(2)
Hg(1)	1.0	0.6394(1)	0.5	0.032(1)	Hg1	0	0.3592	0.5	1.94(5)
Hg(2)	1.0	0.1570(1)	0.5	0.032(1)	Hg2	0	0.8427(3)	0.5	2.04(5)
Hg(3)	1.0	0.4798(1)	1.0	0.025(1)	Hg3	0	0.5229(3)	0	1.45(4)
Ge	0.7658(1)	0.3373(2)	0.7300(1)	0.016(1)	Ge	0.2336(2)	0.6623(3)	0.2712(2)	0.74(7)
S(1)	0.2483(3)	0.9777(4)	0.5402(4)	0.022(1)	S(1)	0.7536(5)	0.0192(8)	0.4588(5)	1.3(2)
S(2)	0.7623(3)	0.4857(5)	0.9223(3)	0.023(1)	S(2)	0.2366(5)	0.5162(8)	0.0796(5)	1.2(2)
S(3)	0.5785(3)	0.1821(4)	0.7409(3)	0.021(1)	S(3)	0.4193(5)	0.8187(7)	0.2609(6)	1.2(2)
S(4)	0.4634(4)	0.6988(4)	0.7445(4)	0.022(1)	S(4)	0.5364(6)	0.2995(7)	0.2574(6)	1.3(2)

[a] U_{eq} is defined as one-third of the trace of the orthogonalized U_{ij} tensor. [b] $B_{eq} = 4/3[a^2\beta_{11} + b^2\beta_{22} + c^2\beta_{33} + ab(\cos \gamma)\beta_{12} + ac(\cos \beta)\beta_{13} + bc(\cos \alpha)\beta_{23}]$. [c] A atom was refined as 80(4)% K and 20% Rb.

and a Ge photodiode was placed at the other. No index matching liquid is required. Frequency doubled radiation at 1.75 μm was collected into the detector. The signal measured by the photodiode was compared to that of a $LiNbO_3$ powder sample. To check the value of the powder technique, control experiments were conducted with known materials in powder form (e.g. $ZnGeP_2$, $AgGaS_2$) and compared to a corresponding $LiNbO_3$ sample.

Results and Discussion

Synthesis. The polar acentric phases described are α-$K_2Hg_3Ge_2S_8$, α-$K_2Hg_3Sn_2S_8$, β-$K_2Hg_3Ge_2S_8$, β-$K_2Hg_3Sn_2S_8$, β-$Rb_2Hg_3Ge_2S_8$, β-$Rb_2Hg_3Sn_2S_8$, and β-$(K,Rb)_2Hg_3Ge_2S_8$. They were prepared using the molten polychalcogenide salt technique of synthesis.[24] α-$K_2Hg_3Ge_2S_8$ and α-$K_2Hg_3Sn_2S_8$ were discovered first and crystallographically determined to have formed with a new structure type. Later, the β-form of potassium, rubidium, and mixed potassium−rubidium analogues were synthesized and determined to have adopted a different but closely related structure type. The stoichiometries of the two types are identical, most of the structural features are common to both, and their physical properties are similar. They are designated α- and β-phases because their space groups are different and also to distinguish them from a third centrosymmetric γ-form of this stoichiometry.

Both α- and β-$K_2Hg_3M_2S_8$ (M = Ge, Sn) have been prepared with a variety of flux compositions and are stable in water and air. The α-$K_2Hg_3M_2S_8$ phases were synthesized at 400 °C, but reactions at higher temperatures form β-$K_2Hg_3M_2S_8$ or mixtures of α- and β-$K_2Hg_3M_2S_8$. We also found that the fraction of the β-form in α-$K_2Hg_3M_2S_8$/β-$K_2Hg_3M_2S_8$ mixtures, synthesized at higher temperatures, increased with reaction time. The centrosymmetric γ-$Rb_2Hg_3M_2S_8$ phases[13] were synthesized at temperatures up to 350 °C, whereas the β-$Rb_2Hg_3M_2S_8$ phases form above that temperature.[25] Interestingly, only the β-form can be stabilized if Rb⁺ replaces all of K⁺. In addition, there are kinetic aspects to the α → β phase transition associated with the length of the reaction time.

Table 3. Dependence of α-/β-$K_2Hg_3Ge_2S_8$ Distribution in Various Synthetic Mixtures as a Function of Flux Composition

total flux composition	T (°C)	time at T	cooling rate (°C/h)	estimated phase content[a] % α	% β
$K_8Hg_4Ge_2S_{40}$	400	4 d	−4	100	
$K_8Hg_4Ge_2S_{40}$	450	4 d	−4	50	50
$K_8Rb_{0.4}Hg_{4.3}Ge_2S_{43}$	400−385	5.5 d	−2	60	40
$K_{6.9}Rb_{1.2}Hg_{4.2}Ge_2S_{40}$	400−385	5.5 d	−2	20	80
$K_{6.2}Rb_{2.1}Hg_4Ge_2S_{42}$	400−385	5.5 d	−2	10	90
$K_{5.6}Rb_{2.4}Hg_4Ge_2S_{40}$	400	4 d	−4		100
$K_{4.8}Rb_{3.2}Hg_4Ge_2S_{40}$	400	4 d	−4		100
$K_8Hg_{3.5}Ge_2S_{35}$	500	45 h	−4	50	50
$K_8Hg_4Sn_2S_{40}$	400	4 d	−4	100	
$K_8Hg_4Sn_2S_{40}$	460	4 d	−4	80	
$K_6Rb_2Hg_{3.5}Sn_2S_{40}$	∼400	4 d	−4	100	

[a] The relative amounts of the α- and β-phases in two-phase samples (as isolated) were estimated from X-ray powder diffraction plots.

β-$Rb_2Hg_3Ge_2S_8$ and β-$Rb_2Hg_3Sn_2S_8$ both form in a flux of an approximate composition "$Rb_8Hg_4M_2S_{40}$" (M = Ge, Sn) at the cool end of a Pyrex tube in a temperature gradient of 450−500 °C. Solid solutions of the type $(K,Rb)_2Hg_3M_2S_8$ synthesized at 400 °C, with at least 25% Rb_2S_x in the flux, are pure β-phase. Below 25% Rb_2S_x, the $(K,Rb)_2Hg_3M_2S_8$ form as α-phase/β-phase mixtures. Table 3 summarizes some relevant information pertaining to the synthesis of these compounds. The observations included in this table and those presented below, suggest that the β-phase is probably the most thermodynamically stable form. In further support of the thermodynamic stability of the β-form, we have observed that α-$K_2Hg_3M_2S_8$ can be prepared as pure phases only in K_2S_x flux reactions, whereas direct combination reactions produce β-$K_2Hg_3M_2S_8$. This conclusion is also supported by the observed optical energy gaps of these materials (see below).

(24) (a) Kanatzidis, M. G. *Curr. Opin. Solid State Mater. Sci.* **1997**, 2, 139. (b) Sutorik, A.; Kanatzidis, M. G. *Prog. Inorg. Chem.* **1995**, 43, 151.
(25) In none of the experiments we performed did we detect the centrosymmetric "γ-$K_2Hg_3M_2S_8$". It would appear that these centrosymmetric potassium compounds are not stable.
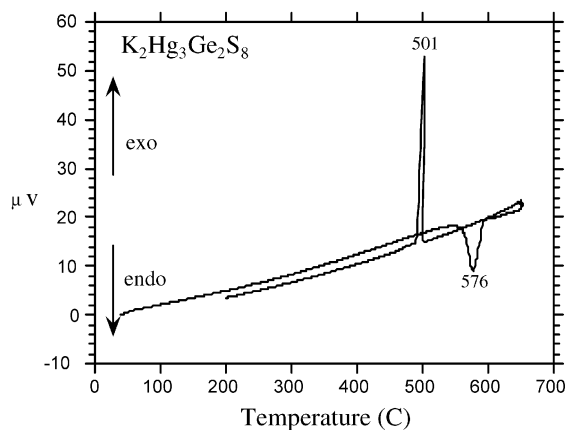
Figure 1. DTA diagram of α-$K_2Hg_3Ge_2S_8$ showing the melting and recrystallization events.

Thermal Properties, Crystal Growth, and Solubility of $K_2Hg_3Ge_2S_8$ in K_2S_8 Flux. DTA experiments indicate that all $K_2Hg_3M_2S_8$ phases melt incongruently. Repeated heating and cooling cycles show reproducible melting endothermic and recrystallization exothermic events. Care must be taken to minimize thermal gradients within the sample containers, because the Hg in these materials is relatively labile and large temperature gradients allow HgS to volatilize away from the $K_2Hg_3M_2S_8$ phase. The remaining material is a mixture of $K_2Hg_3M_2S_8$ and other phases, some of which are water-soluble (presumably molecular K−Sn−S type compounds). $K_2Hg_3Sn_2S_8$ is more susceptible to this partial decomposition than $K_2Hg_3Ge_2S_8$. While molten, some HgS begins to evaporate from the surface and can cause complications in crystal growth experiments if attempted from the stoichiometric melt. Despite this, we believe it should be possible to grow crystals from a stoichiometric melt by suppressing this evaporation under an overpressure of inert gas over the sample. The recrystallized material was invariably β-phase, regardless of whether the starting composition was α- or β-phase or a mixture of the two.

The pure phases α-$K_2Hg_3Ge_2S_8$ and α-$K_2Hg_3Sn_2S_8$ show melting points of ∼576 and ∼545 °C and recrystallization points of ∼501 and ∼430 °C, respectively. A representative DTA diagram showing these thermal events is shown in Figure 1.

Recrystallization from K_2S_8 Flux. The melting and recrystallization temperatures of α-$K_2Hg_3M_2S_8$/K_2S_x mixtures vary as expected with the ratio of the two components. The melting/recrystallization data, shown in Figure 2, provided valuable solubility data of α-$K_2Hg_3M_2S_8$ in the flux that can be used to determine heating and cooling profiles for crystal growth studies of these materials both with and without K_2S_x flux present. Significant supercooling appears to be present, as seen in the large differences between dissolution and recrystallization temperatures.[26] This is the first time data of this type have been obtained for systems grown in polychalcogenide flux. In addition to being useful in helping to grow crystals of these phases, such data are rare to obtain and are relevant to understanding the role polychalcogenide fluxes generally play in promoting formation and crystallization of various compounds.

(26) Other DTA experiments using 1:2, 1:1, and 2:1 ratios exhibit broad melting endotherms and sharper recrystallization exotherms. As the reaction mixtures become more dilute, the recrystallizations become broad. Substantial supercooling appears to occur, i.e., the difference between dissolution and recrystallization temperatures is large.
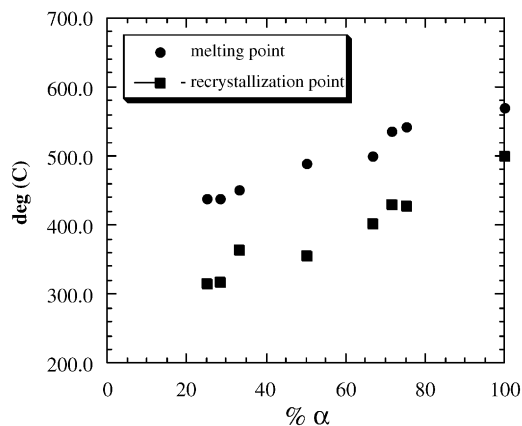
Figure 2. Variation in melting and recrystallization points of a mixture of α-$K_2Hg_3Ge_2S_8$ and K_2S_8 as a function of α-fraction.

Recrystallization using a 1:1 α-$K_2Hg_3M_2S_8$/K_2S_8 ratio worked best for crystal growth in terms of size and optical quality. The ratios from 2:3 to 3:2 also work well. The composition of the flux can range from K_2S_3 up to at least K_2S_{16}. The more sulfur-rich fluxes result in copious elemental sulfur, whereas the more basic fluxes (K-rich) result in poor crystallinity and/or other phases. Good optical quality crystals (α-) resulted from 1:1 reactions, which were kept at 530 °C for >3 d and cooled in cycles (slow cool for 100 °C/heat back up for 75 °C) down to 350 °C. Presumably everything is in solution at 530 °C and most of the material has crystallized when cooled to 350 °C. Greater than 85% yield of $K_2Hg_3Ge_2S_8$ could be isolated from reactions slow-cooled to 200 °C, while only 62% could be isolated from those cooled to 400 °C. When a reaction tube was removed from the furnace at 450 °C (i.e. quenching), it did not contain crystals upon isolation, indicating that the 1:1 mixture was a solution at this temperature. These observations suggest that crystal growth occurs on cooling.

The best crystals so far for α-$K_2Hg_3Ge_2S_8$ were obtained from a procedure involving temperature oscillation, where a 1:1 α-$K_2Hg_3M_2S_8$/K_2S_8 reaction mixture was heated to 530 °C (resulting in complete dissolution of the compound) and then slowly cooled 430 °C followed by heating to 505 °C and then down to 350 °C. These results are reproducible, and reasonably sized optical quality crystals (up to about 1 mm³) could be obtained. These crystals were then used in measuring the NLO properties described below.

Description of Structures. α-Form. Compounds α-K_2Hg_3-Ge_2S_8 (**I**) and α-$K_2Hg_3Sn_2S_8$ (**II**) are isostructural orthorhombic phases that belong to the *Aba*2 space group. We will focus our discussion on the Ge analogue and make references to the Sn compound where appropriate. The polar character of the structure of $K_2Hg_3Ge_2S_8$ is evident when viewed down the *b*-axis (see Figure 3A). The structure can be described in terms of a three-dimensional covalent anionic $[Hg_3Ge_2S_8]^{2-}$ framework filled with K⁺ ions. There are two types of Hg²⁺ atoms, a highly distorted tetrahedral [Hg(2) "seesaw-shaped" HgS₄] and a linearly coordinated Hg(1) atom. The former type features two short Hg(2)−S(3) and Hg(2)−S(4) bonds at 2.406(9) and 2.413(9) Å and two longer bonds Hg(2)−S(1) at 2.787(8) and 2.845(9) Å (see Figure 4A). The $[GeS_4]^{4-}$ tetrahedra act as ligands coordinating to the Hg²⁺ ions to form the framework. More specifically, they share corners with the seesaw-shaped Hg-centered tetrahedra to form layers of the stoichiom-

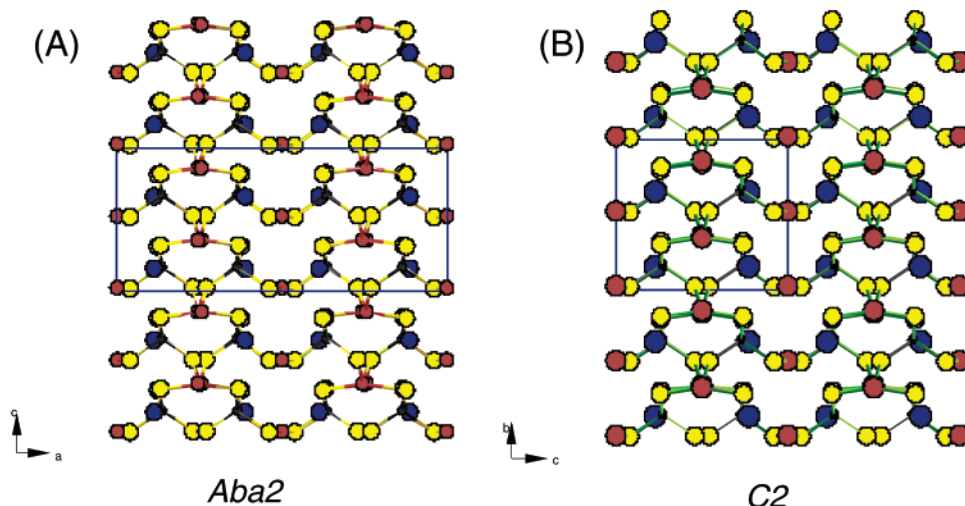**Figure 3.** Crystal structure of (A) α-K₂Hg₃Ge₂S₈, (s.g. *Aba*2). (B) Crystal structure of β-K₂Hg₃Ge₂S₈, (s.g. *C*2). Blue circles are K, red circles are Hg, black circles are Ge, and yellow circles are S atoms.
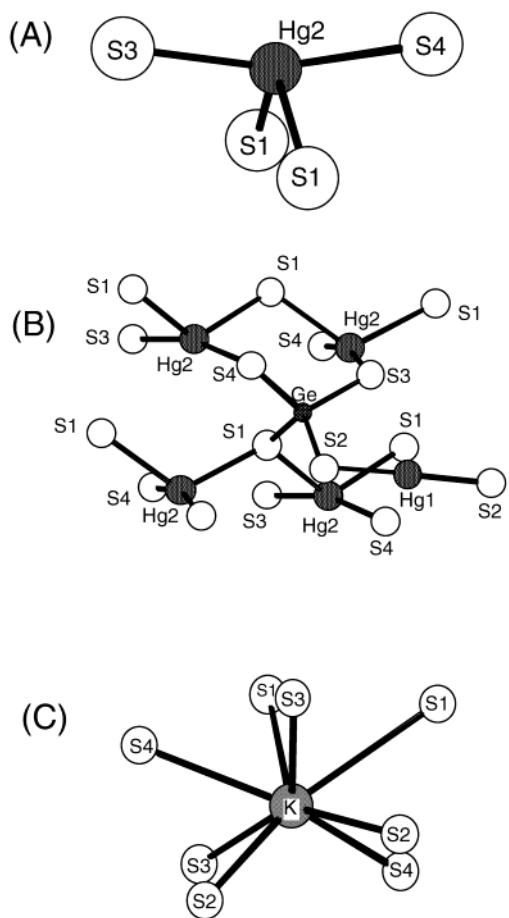

Figure 4. (A) The highly distorted "see-saw" type coordination of Hg(2) atoms. (B) Large fragment from the α-K₂Hg₃Ge₂S₈ structure showing the vicinity of the [GeS₄]⁴⁻ anion. (C) The immediate coordination environment of the K⁺ ions.

etry [Hg₂Ge₂S₈].⁴⁻ The immediate coordination environment of the thiogermanate anion is shown in Figure 4B. The [Hg₂Ge₂S₈]⁴⁻ layers are then linked in the third direction via the linearly coordinated Hg(1) atoms to produce the polar three-dimensional framework (see the polyhedral representation in Figure 5A). Interestingly, if the two long Hg(2)−S(1) bonds of the seesaw-like HgS₄ units are ignored, the three-dimensional
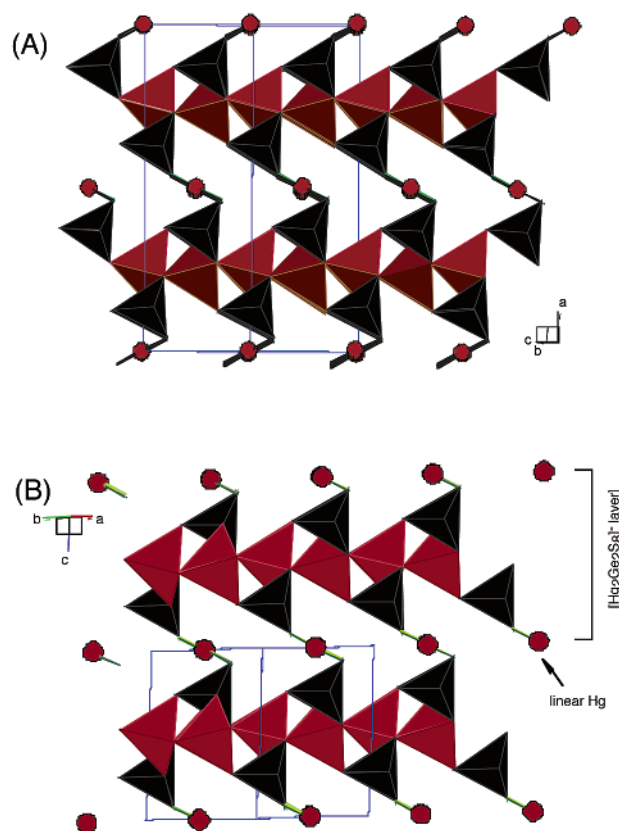

Figure 5. Polyhedral representation of the structure of (A) α-K₂Hg₃Ge₂S₈ and (B) β-K₂Hg₃Ge₂S₈ showing the bridging role of the linearly coordinated Hg atoms.

framework becomes a two-dimensional sheet parallel to the *ab*-plane.

The K⁺ ions are surrounded by six [GeS₄]⁴⁻ tetrahedra positioned in an octahedral fashion. The sulfur atom cage that defines the K⁺ ion environment, however, has a bicapped trigonal-prismatic outline shown in Figure 4C. A comparison of the selected bond distances and angles between **I** and **II** is given in Table 4.

β-Form. The isostructural monoclinic β-K₂Hg₃Ge₂S₈ (**III**) and β-K₂Hg₃Sn₂S₈ (**IV**) differ only slightly from the α-form.

Table 4. Comparison of Selected Bond Distances (Å) and Angles (deg) of α-K$_2$Hg$_3$Ge$_2$S$_8$(**I**) and α-K$_2$Hg$_3$Sn$_2$S$_8$(**II**)

	I	II		I	II
		Selected Bond Distances (Å)			
Hg(1)−S(2) × 2	2.333(8)	2.347(3)	mean M−S	2.202(9)	2.390(3)
Hg(2)−S(1)	2.787(8)	2.798(3)	K−S(1)	3.206(13)	3.197(5)
Hg(2)−S(1)	2.845(9)	2.853(4)	K−S(2)	3.144(12)	3.399(6)
Hg(2)−S(3)	2.406(9)	2.420(4)	K−S(2)	3.324(14)	3.213(5)
Hg(2)−S(4)	2.413(9)	2.439(3)	K−S(3)	3.316(12)	3.297(5)
M−S(1)	2.143(10)	2.345(4)	K−S(3)	3.342(12)	3.462(6)
M−S(2)	2.241(9)	2.417(3)	K−S(4)	3.158(12)	3.197(5)
M−S(3)	2.212(9)	2.402(3)	K−S(4)	3.426(11)	3.526(5)
M−S(4)	2.211(9)	2.396(3)	mean K−S	3.274(12)	3.327(5)
		Selected Bond Angles (deg)			
S(2)−Hg(1)−S(2)	177.5(5)	177.5(2)	S(2)−M−S(3)	107.6(3)	107.35(12)
S(1)−Hg(2)−S(1)	118.4(4)	123.18(16)	S(2)−M−S(4)	102.9(3)	104.87(11)
S(1)−Hg(2)−S(3)	91.9(3)	98.83(10)	S(3)−M−S(4)	112.9(4)	113.06(13)
S(1)−Hg(2)−S(4)	89.5(3)	88.75(10)	Hg(1)−S(2)−M	99.3(3)	98.10(12)
S(1)−Hg(2)−S(3)	91.9(3)	91.38(11)	Hg(2)−S(3)−M	101.6(3)	99.86(13)
S(1)−Hg(2)−S(4)	94.8(3)	93.32(10)	Hg(2)−S(4)−M	103.0(4)	101.73(12)
S(3)−Hg(2)−S(4)	163.6(3)	167.9(1)	Hg(2)−S(1)−Hg(2)	116.1(4)	121.46(16)
S(1)−M−S(2)	113.4(4)	112.52(15)	Hg(2)−S(1)−M	110.8(3)	109.10(12)
S(1)−M−S(3)	110.5(3)	110.33(12)	Hg(2)−S(1)−M	115.1(3)	113.15(12)
S(1)−M−S(4)	109.4(4)	108.65(12)			
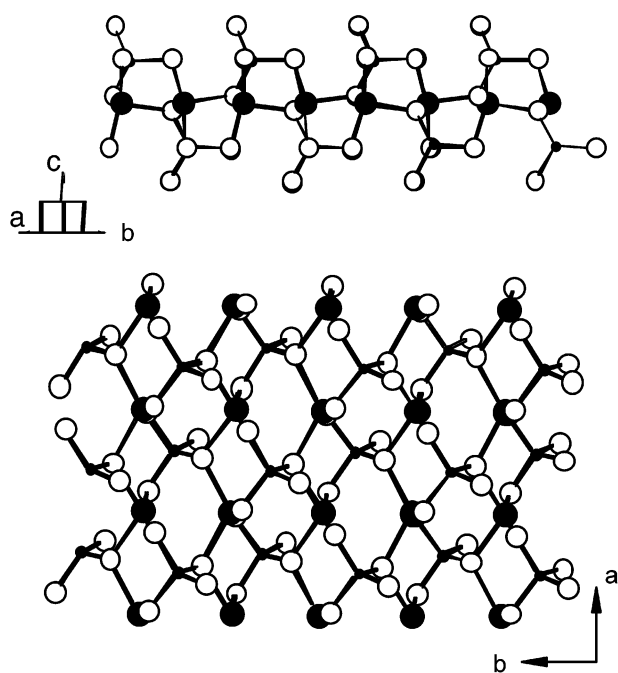
Figure 6. Two views (parallel and perpendicular) of the slabs of [Hg$_2$Ge$_2$S$_8$]$^{4-}$, β-form. These slabs are linked in the third direction by the linear Hg(1) atoms.

Table 5. Selected Bond Distances (Å) and Angles (deg) of β-K$_2$Hg$_3$Ge$_2$S$_8$ (**III**)

		Selected Bond Distances (Å)	
Hg(1)−S(2) × 2	2.341(3)		
Hg(2)−S(1) × 2	2.813(3)	K−S(1)	3.188(5)
Hg(2)−S(4) × 2	2.439(4)	K−S(2)	3.236(5)
Hg(3)−S(3) × 2	2.412(3)	K−S(2)	3.376(5)
Hg(3)−S(1) × 2	2.819(3)	K−S(3)	3.179(5)
Ge−S(1)	2.171(4)	K−S(3)	3.415(5)
Ge−S(2)	2.235(3)	K−S(4)	3.311(5)
Ge −S(3)	2.224(3)	K−S(4)	3.415(5)
Ge −S(4)	2.215(4)	mean K−S	3.303(5)
mean M−S	2.211(4)		
		Selected Bond Angles (deg)	
S(2)−Hg(1)−S(2)	177.6(2)	S(4)−Ge−S(3)	112.5(1)
S(4)−Hg(2)−S(4)	163.6(3)	S(1)−Ge−S(2)	113.3(1)
S(4)−Hg(2)−S(1)	91.3(1)	S(4)−Ge−S(2)	107.9 (1)
S(4)−Hg(2)−S(1)	97.4(1)	S(3)−Ge−S(2)	102.6 (1)
S(1)−Hg(2)−S(1)	115.6(2)	Hg(2)−S(3)−Ge	103.3(1)
S(3)−Hg(3)−S(3)	163.0(2)	Hg(2)−S(4)−Ge	101.7(1)
S(3)−Hg(3)−S(1)	98.2(1)	Hg(1)−S(2)−Ge	100.1(1)
S(3)−Hg(3)−S(1)	90.0(1)	Hg(2)−S(1)−Hg(3)	116.8(1)
S(1)−Hg(3)−S(1)	122.8(2)	Hg(2)−S(1)−Ge	114.3(1)
S(1)−Ge−S(4)	110.1(1)	Hg(3)−S(1)−Ge	111.5(1)
S(1)−Ge−S(3)	110.3(3)		

Their framework structures are very similar to those of **I** and **II** and are made up with tetrahedral MS$_4$ (M = Ge, Sn) units, linear HgS$_2$, and "seesaw-like" HgS$_4$ moieties (Figures 3B and 5B). Specific metric details will refer to the Ge analogue for which a superior refinement was obtained. The structures of **III** and **IV** are also polar, as can be readily seen by the fact that all S(1)−Hg(2)−S(1) and S(3)−Ge−S(4) angles point in the same direction, [010]. In this case too, if the two long Hg(2)−S(1) bonds of the seesaw-like units are ignored, the three-dimensional framework can be simplified to a layered one (Figure 6). The γ-form of Rb$_2$Hg$_3$Sn$_2$S$_8$ and Rb$_2$Hg$_3$Ge$_2$S$_8$ have a three-dimensional [Hg$_3$M$_2$S$_8$]$^-$ framework, which incidentally also features a "seesaw-like" HgS$_4$ moiety and linear S−Hg−S fragments.[14]

Selected bond distances and angles for **III** are given in Table 5. The average Ge−S distance is normal at 2.211(3) Å. The S−Ge−S angles are close to those of a perfect tetrahedron. There are three distinct Hg atoms in the structure. Hg(1) adopts linear coordination with the Hg(1)−S(2) distances at 2.341(3) Å and S(2)−Hg(1)−S(2) angles at 177.6(2)° for **III**. Hg(2) and Hg(3) are four-coordinated and adopt a saddle-like geometry (as in the α-form), which has two short and two long Hg−S bonds, the former averaging 2.426(4) Å and the latter averaging 2.816(3) Å. The saddle-like geometry derives by severely distorting a tetrahedron and results in one very large S−Hg−S angle. For Hg(2) and Hg(3) the angles between the two short Hg−S bonds are 163.6(2)° and 163.0(2)°. The two short Hg−S bond distances fall between those in normal linear HgS$_2$ (ca. 2.35 Å) and tetrahedral HgS$_4$ (ca. 2.55 Å) geometries. Therefore, the coordination geometry of Hg(2) and Hg(3) may be considered as intermediate between tetrahedral HgS$_4$ and linear HgS$_2$, having short contacts with two S atoms. This coordination type

of HgS_4 is novel and has not been observed in other thiomercurates. The angles around the Hg atoms are given in Table 5. The K^+ cations in **III** are surrounded by seven sulfur atoms with average $K^+\cdots S$ distances of 3.303(5) Å.

The existence and structural differences of the centrosymmetric two-dimensional $Cs_2Hg_3M_2S_8$ and three-dimensional γ-$Rb_2Hg_3M_2S_8$ (M = Ge, Sn) have been discussed previously in terms of the cation size effect.[27] The formation of α-K_2Hg_3-Ge_2S_8 (**I**), α-$K_2Hg_3Sn_2S_8$ (**II**), β-$K_2Hg_3Ge_2S_8$ (**III**), β-K_2Hg_3-Sn_2S_8 (**IV**), β-$Rb_2Hg_3Ge_2S_8$ (**V**), β-$Rb_2Hg_3Sn_2S_8$ (**VI**), and β-$(K,Rb)_2Hg_3Ge_2S_8$ (**VII**) are additional examples of the cation size effect. Thus, while the $[Hg_3M_2S_8]^{2-}$ framework forms layers with the large Cs^+ cations, the smaller K^+ and Rb^+ prefer a more condensed three-dimensional arrangement. What is not well understood is why the K^+ atoms strongly favor the polar α- or β-structures, whereas the Rb^+ analogues which can adopt either β- or γ-types.

The structural framework differences between the α-, β-, and γ-phases are subtle. For example, the arrangement within the $[Hg_2Ge_2S_8]^{4-}$ layers is the same, but the difference lies in how the linearly coordinated Hg^{2+} ions bridge them into a framework. The direction of the linear S—Hg—S bridge in the two forms (α-, β-) is opposite with respect to the $[Hg_2Ge_2S_8]^{4-}$ layers, as shown in Figure 7. In each case the Hg^{2+} ion selects two S atoms, one from each layer to form the bridge. However, whereas the S—Hg—S coordination is linear in each case, the pairs of S atoms involved from each layer are different, giving rise to the two forms. Energetically there appears to be very little difference, since the number and type of Hg—S bonds in the bridge are the same. This could explain the existence of both forms and their relative ease of transformation. The transformation may be readily envisioned to occur by a small sliding of the $[Hg_2Ge_2S_8]^{4-}$ layers about the linear Hg atoms. The dashed lines in Figure 7 are intended to indicate the new set of Hg—S bonds that would result upon layer sliding that is necessary to convert one form to the other.

Thermal Expansion of α-$K_2Hg_3Ge_2S_8$. To obtain more information about the liquid-to-crystal transition during crystallization of such a melt, and to evaluate the potential for cracks in the growing crystal, it is useful to know the thermal expansion coefficient of the solid. Therefore, the lattice parameters of a single crystal of α-$K_2Hg_3Ge_2S_8$ were measured as a function of temperature using an X-ray diffractometer. Plots of thermal expansion of the *a*, *b*, and *c* parameters as well as the resulting coefficients are shown in Figure 8. The thermal expansion is somewhat anisotropic for $K_2Hg_3Ge_2S_8$, ranging from values close to that of ordinary glass ($a_L = 0.52 \times 10^{-5}/K$ *a*-axis) to values close to that of lead ($a_L = 3.36 \times 10^{-5}/K$ *c*-axis). It is also interesting to note that the single crystals never cracked or showed any signs of wear when exposed to abrupt changes in temperature.

Energy Gaps, Infrared Spectra, and NLO Properties. The UV/vis/near-IR spectra of all $A_2Hg_3M_2S_8$ compounds described here exhibit steep absorption edges associated with optical band gap transitions. Therefore, the compounds are wide-gap semiconductors. α-$K_2Hg_3Ge_2S_8$ has a band gap of 2.64 eV and β-$K_2Hg_3Ge_2S_8$ has 2.70 eV, consistent with their pale yellow

(27) (a) Kanatzidis M. G. *Phosphorous, Silicon Sulfur* **1994**, *93−94*, 159−172. (b) Kim K.-W.; Kanatzidis M. G. *J. Am. Chem. Soc.* **1998**, *120*, 8124−8135.
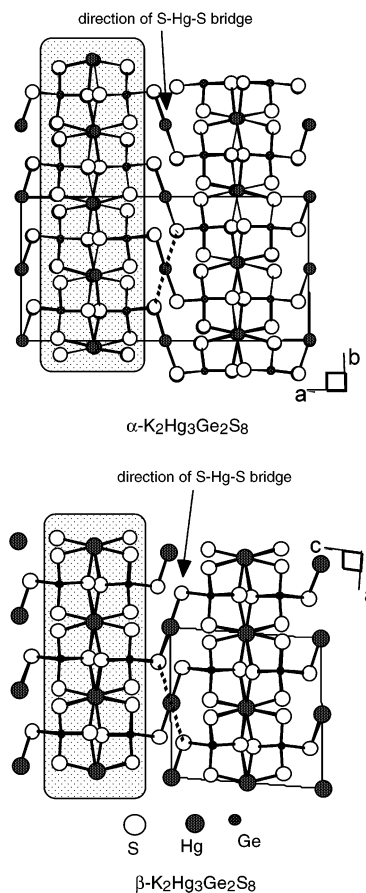

Figure 7. Comparison of the two $[Hg_3Ge_2S_8]^{2-}$ frameworks (α- and β-) showing the subtle difference in the bridging mode of the linear Hg atoms. Both frameworks have the same type of $[Hg_2Ge_2S_8]^{4-}$ layers (indicated by boxed shaded areas), but the difference lies in which set of S atoms pairs are joined by the linking Hg atoms. The dashed lines indicate the hypothetical alternate S—Hg—S bonding that occurs in the opposite form. A α → β conversion may occur via a small amount of sliding of layers.

color. The Sn analogues have more narrow gaps at 2.40 and 2.50 eV (deep yellow) for α- and β-form, respectively. The slightly large energy gap of the β-form in both the Ge and Sn cases is also consistent with the slightly higher thermodynamic stability of this form, as discussed above. The energy of the transitions depends strongly on M and weakly on A. Typical spectra are shown in Figure 9. The band gaps are given in Table 6. It is important to note that below the band gap transition there is very little light absorption, suggesting the absence of impurities and uninterrupted light transmission through these materials. This property is key to explore and exploit the NLO properties of these materials. The spectral transmission of $K_2Hg_3Ge_2S_8$ is similar to that of $AgGaS_2$. The material is transparent from ~500 nm to over 10 μm (see Figure 10). We expect that the substitution of Se for S will extend the LWIR transmission well past 12 μm, just as in $AgGaSe_2$.

The infrared spectra for $K_2Hg_3Ge_2S_8$ and $K_2Hg_3Sn_2S_8$ (β-forms) exhibit a complex set of absorption frequencies due to many possible vibrational modes. All the absorption frequencies fall in the range between 130 and 450 cm⁻¹, because they are isostructural, and the vibrational spectra of the two compounds have similar patterns, except that all absorption bands of $K_2Hg_3Ge_2S_8$ lie understandably at higher frequencies. For $K_2Hg_3Sn_2S_8$, the absorptions occur at 383 (s), 356 (sh), 345
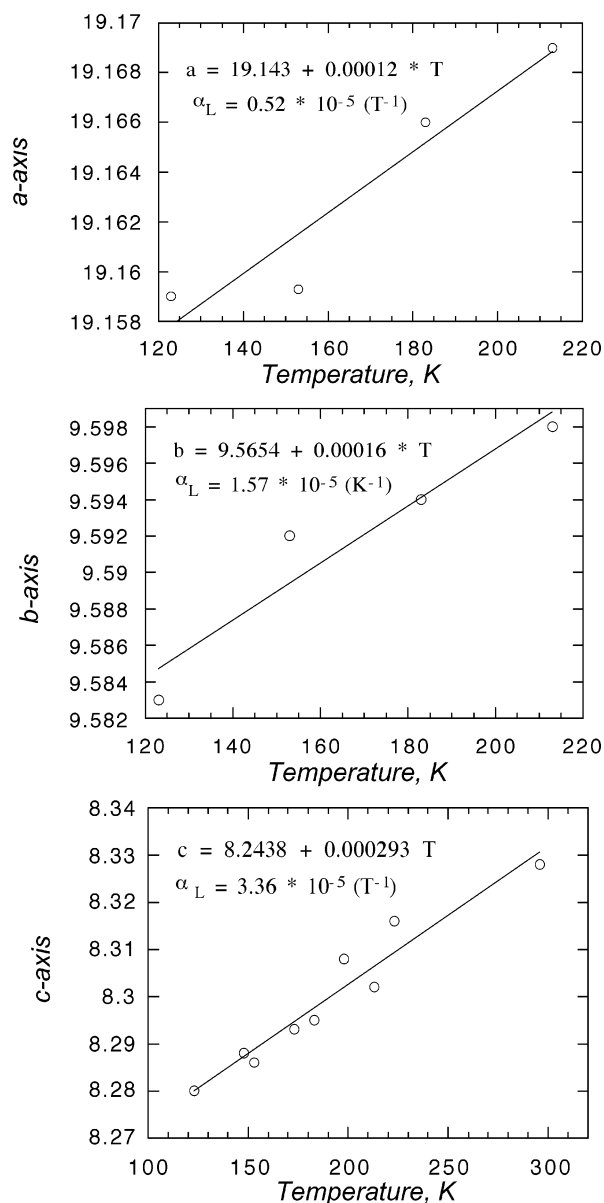
Figure 8. Temperature variation of the lattice parameters of α-K$_2$Hg$_3$-Ge$_2$S$_8$ revealing anisotropic thermal expansion. The expansion coefficients are given in the insets.

(s), 316 (w), 296 (m), 169 (m) cm^{-1}, whereas for K$_2$Hg$_3$Ge$_2$S$_8$ they lie at 421 (s), 393(m), 377 (s), 371 (sh), 353 (m), 312 (m), 297 (sh), 211 (sh), 198 (s), 148 (w), 134 (w) cm^{-1}.

Currently available NLO materials for SHG and related applications in the midwave infrared (MWIR) and long-wave infrared (LWIR) lack one (or more) of the following desired properties: a large nonlinear coefficient, wide-band spectral transparency, low absorption loss at convenient pump-laser wavelengths, high laser-damage threshold, reasonable chemical stability, good mechanical robustness, high thermal conductivity, low thermal index change, or birefringently phase-matched over an appropriate wavelength regime. A zinc blende semiconductor such as GaAs with its tetrahedral coordination has a very large nonlinear coefficient ($d_{14} \sim 150$ pm/V), but its cubic symmetry dictates no birefringence; consequently, second-order NLO processes cannot be phase-matched (except through quasiphase matching). Chalcopyrite semiconductors (including ZnGeP$_2$,
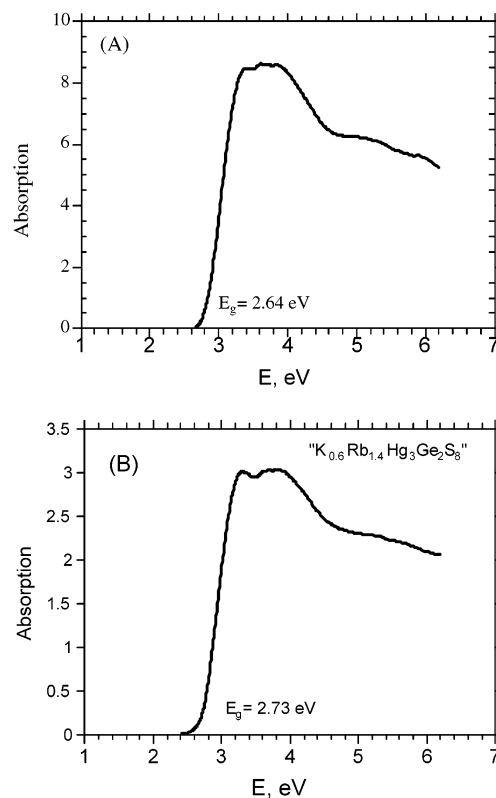
Figure 9. Optical absorption spectra of (A) α-K$_2$Hg$_3$Ge$_2$S$_8$ and (B) β-K$_{0.6}$-Rb$_{1.4}$Hg$_3$Ge$_2$S$_8$

Table 6. Summary of Spectroscopically Determined Energy Gaps of the Various A$_2$Hg$_3$M$_2$S$_8$ Analogs

compound	band gap, eV	compound	band gap, eV
α-K$_2$Hg$_3$Ge$_2$S$_8$	2.64	β-Rb$_2$Hg$_3$Ge$_2$S$_8$	2.80
α-K$_2$Hg$_3$Sn$_2$S$_8$	2.40	β-Rb$_2$Hg$_3$Sn$_2$S$_8$	2.48
β-K$_2$Hg$_3$Ge$_2$S$_8$	2.70	β-K$_{0.6}$Rb$_{1.4}$Hg$_3$Ge$_2$S$_8$	2.73
β-K$_2$Hg$_3$Sn$_2$S$_8$	2.50	β-K$_{0.8}$Hg$_{1.2}$Sn$_2$S$_8$	2.78

Figure 10. IR/near-IR/vis transmission spectrum for a single crystal of α-K$_2$Hg$_3$Ge$_2$S$_8$.

AgGaS$_2$, AgGaSe$_2$, and CdGeAs$_2$) have a similar tetrahedrally coordinated covalent bonding and also exhibit large optical nonlinearities (e.g., ranging from 13 pm/V in AgGaS$_2$ to 235 pm/V in CdGeAs$_2$).[28] Their tetragonal symmetry provides the

(28) Dmitriev, V. G.; Gurzadyan, G. G.; Nikogosyan, D. N. *Handbook of Nonlinear Optical Crystals*; Springer-Verlag: Berlin, 1991.
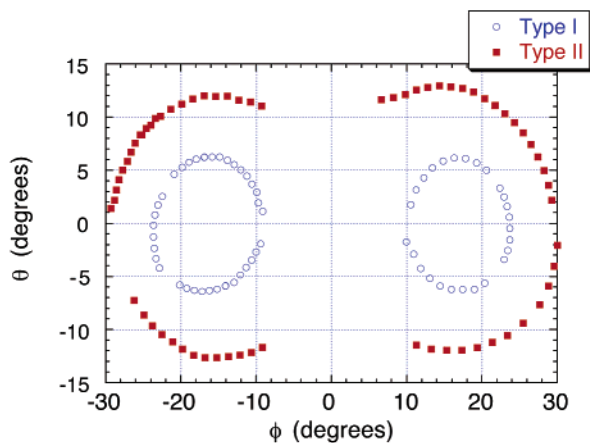
Figure 11. Direct phase-matching loci for type I and type II SHG in single crystal β-K$_2$Hg$_3$Ge$_2$S$_8$.

Figure 12. Phase-matched SHG signal observed for β-K$_2$Hg$_3$Ge$_2$S$_8$ (relative to LiNbO$_3$ SHG).

necessary birefringence to make them phase-matchable. However, restricted transmission ranges, extrinsic absorptions, and poor thermal properties (e.g. ZnGeP$_2$ and CdGeAs$_2$) sometimes limit the usefulness of these materials for frequency conversion, particularly when a Nd:YAG laser is desired as the pump source.

The polar, noncentrosymmetric structures of the α- and β-forms reported here coupled with the extensive covalent bonding between the easily polarizable Ge, S, and Hg atoms should lead to large optical nonlinearities. First we screened all compounds as polycrystalline powders qualitatively for SHG using a Nd-doped YAG laser operating in the near-infrared at 1064 nm. When exposed to this wavelength, all samples emitted green light (at 532 nm), clearly demonstrating frequency-doubling NLO behavior. Because of these observations, we carried out more quantitative measurements on crystals of the β-form.

We have ascertained the frequency conversion characteristics of β-K$_2$Hg$_3$Ge$_2$S$_8$ in the MWIR from SHG. The 3.5 μm idler beam from an optical parametric oscillator was focused into a small single-crystal microsphere (~1 mm diameter); the SHG signal at 1.75 μm was observed when the microsphere is angularly oriented to satisfy the phase-matching condition (conservation of momentum). This method for measuring direct phase-matched (DPM) SHG has been described elsewhere.[29,30] The DPM experiment in the MWIR yields the nonlinear coefficient d_{eff} and the angular sensitivity for β-K$_2$Hg$_3$Ge$_2$S$_8$ at each point on the phase-matching locus. Both the type I and type II phase-matched SHG were observed, and the phase-matching loci are shown in Figure 11. The variation in SHG signal for β-K$_2$Hg$_3$Ge$_2$S$_8$ along each phase-matching locus (relative to the maximum type I SHG signal measured in a plate of LiNbO$_3$ with differences in crystal interaction lengths taken into account) is shown in Figure 12. At the optimal propagation directions, the SHG signals from both type I and type II phase matching in β-K$_2$Hg$_3$Ge$_2$S$_8$ are about a factor of 10 larger than

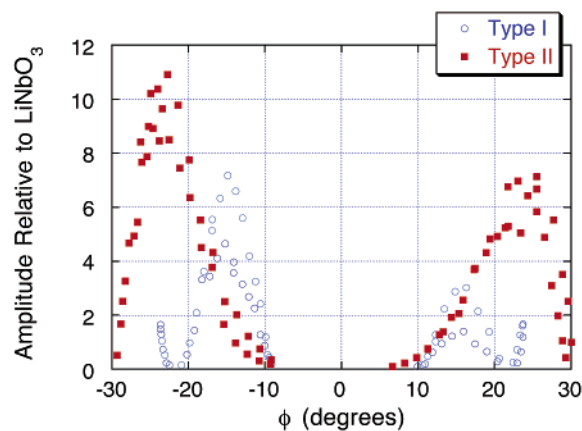that in LiNbO$_3$, corresponding to d_{eff} values for K$_2$Hg$_3$Ge$_2$S$_8$ approaching 20 pm/V (Figure 12). This value is significantly larger than that of the commercially available material AgGaS$_2$. Beam intensities as high as 30 MW/cm^2 were used in these DPM experiments with K$_2$Hg$_3$Ge$_2$S$_8$, thereby providing a lower bound for the laser-damage threshold in K$_2$Hg$_3$Ge$_2$S$_8$.

Concluding Remarks

Exploratory solid-state chemistry with polychalcogenide fluxes has produced the large family of materials A$_2$Hg$_3$M$_2$S$_8$ (A = alkali metal; M = Ge, Sn).[14] From this the members K$_2$Hg$_3$M$_2$S$_8$ and Rb$_2$Hg$_3$M$_2$S$_8$ are an interesting subgroup of strongly polar acentric semiconductors. The polar compounds come in two closely related orthorhombic (α-) and monoclinic (β-) forms, both exhibiting high environmental stability, optical transparency, and good NLO response. Relatively large (larger than a millimeter on edge) optical-quality pieces of K$_2$Hg$_3$Ge$_2$S$_8$ crystals can be synthesized by recrystallization using slow cooling and/or temperature cycling of K$_2$Hg$_3$Ge$_2$S$_8$/K$_2$S$_8$ flux reactions. We believe larger crystals can be grown using variations of these techniques. Crystal growth starting from seeds should be considered, because that would diminish supercooling, which results in rapid recrystallization and presumably leads to poor crystal quality, particularly of the crystal cores. In addition to the large second-order NLO tensor coefficients, which is 10 times larger than that of LiNbO$_3$, these materials (particularly β-K$_2$Hg$_3$Ge$_2$S$_8$) present good birefringence, good mechanical and thermal characteristics, and a high optical damage threshold. Its NLO coefficients exceed those of the commercially available AgGaS$_2$, and as a result, β-K$_2$Hg$_3$Ge$_2$S$_8$ promises to be suitable for a variety of long-wavelength NLO applications.

Supporting Information Available: X-ray crystallographic data (cif files for compounds **I**, **II**, **III**, and **VII**). This material is available free of charge via the Internet at htpp://pubs.acs.org.

(29) Velsko, S. P. Direct measurements of phase matching properties in small single crystals of new nonlinear materials. *Opt. Eng.* **1989**, *28*, 76.
(30) Rosker, M. J.; Cunningham, P.; Ewbank, M. D.; Marcy, H. O.; Vachss, F. R.; Warren, L. F.; Gappinger, R.; Borwick, R. Salt-based approach for frequency conversion materials. *Pure Appl. Opt.* **1996**, *5*, 667.

JA034121L